Thermally induced dephasing of high power second harmonic generation in MgO: $LiNbO_3$ waveguides

Guohui Li (李国辉) and Xinye Xu (徐信业)*

State Key Laboratory of Precision Spectroscopy and Department of Physics, East China Normal University, Shanghai 200062, China

**Corresponding author: xyxu@phy.ecnu.edu.cn*

Received May 4, 2011; accepted August 3, 2011; posted online November 1, 2011

High power second harmonic generation (SHG) in MgO-doped $LiNbO_3$ waveguides is investigated using a three-dimensional (3D) coupled thermo-optical model. Simulations performed for a 1 111.6-nm fundamental laser show the influence of the absorptions and the thermally induced dephasing on the conversion efficiencies of the different waveguides. The onset of the thermally induced dephasing effect for each waveguide is also indicated. As a result of high light intensity in the waveguide, nonlinear absorptions are identified as the possible main factors in efficiency losses in specific cases.

OCIS codes: 190.2620, 190.4870, 190.4390.

doi: 10.3788/COL201109.121901.

Second harmonic generation (SHG) has numerous important applications in nonlinear optics, quantum optics, optical communication, etc.[1−5]. One of its applications is the provision of blue and green laser light sources with greater efficiency and higher power which cannot be generated directly by diode lasers. High power SHG has been studied in various periodically poled bulk crystal devices[6−8]. However, several problems, such as non-uniformity and nonlinear drive, among others have affected the achievement of highly efficient SHG in single-pass bulk interactions. SHG waveguide devices can circumvent these problems[1]. Tight confinement of the interacting waves in the transverse direction provided by a waveguide considerably increases the optical intensity in a small area. Thus, normalized efficiency in a waveguide can be increased significantly. Highly efficient SHG has been demonstrated in the periodically poled lithium niobate (PPLN) waveguide[1,2]. However, the high power SHG in the PPLN waveguide is limited by such effects as photorefractive damage and green-induced infrared absorption (GRIIRA). These problems can be addressed by MgO doping to the $LiNbO_3$ crystal[9]. Therefore, periodically poled MgO-doped $LiNbO_3$ (PPMgLN) is a promising candidate for PPLN in SHG and optical parametric oscillation[10,11]. Highly efficient single-pass SHG has been obtained in PPMgLN waveguide[3−5]. Unfortunately, the problem of efficiency loss has been observed in the fundamental light power of 0.2 W[3]. The saturation of the blue power has been observed in the incident infrared powers higher than 0.9 W[5]. However, the results of theoretical investigations of these problems have not been reported.

In this letter, the optical problem of SHG in the 5 mol % MgO-doped $LiNbO_3$ waveguides coupled with the three-dimensional (3D) steady-state heat transfer equations is considered. The simulations are performed for a 1 111.6-nm fundamental laser. Considering that the waveguides fabricated under different conditions have different optical absorption properties, four PPMgLN waveguides are investigated. The efficiency loss mainly results from the absorptions and thermally induced dephasing in the high fundamental power regime.

The electric field profiles of the fundamental field E_ω and the SHG field $E_{2\omega}$ in the waveguide are $E_\omega(x,y,z,t) = (\gamma_\omega/2)e_\omega(x,y)\{A_\omega(z,t)\exp[\mathrm{j}(\omega t - k_\omega z)] + c.c.\}$ and $E_{2\omega}(x,y,z,t) = (\gamma_{2\omega}/2)e_{2\omega}(x,y)\Big\{A_{2\omega}(z,t)\exp[\mathrm{j}(2\omega t - k_{2\omega}z)] + c.c.\Big\}$, where k_i (i=ω, 2ω) is the modal propagation constant, $e_i(x,y)$ is the transverse modal profile, and $\gamma_i = \sqrt{2/n_i c\varepsilon_0}$ is a normalization constant, where n_i is the refractive index, ε_0 is the permittivity of free space, and c is the *in vacuo* speed of light[12]. The envelope function A_i is normalized to satisfy the power in each mode $P_i = |A_i|^2$.

The SHG in the waveguide can be described by the coupled mode equations[1,6]:

$$\frac{\mathrm{d}A_\omega}{\mathrm{d}z} = -\mathrm{j}\sqrt{\eta_0}A_\omega^* A_{2\omega}\exp(-\mathrm{j}\Delta k z) - \alpha_\omega A_\omega, \quad (1)$$

$$\frac{\mathrm{d}A_{2\omega}}{\mathrm{d}z} = -\mathrm{j}\sqrt{\eta_0}A_\omega^2\exp(\mathrm{j}\Delta k z) - (\alpha_{2\omega} + \beta I_{2\omega})A_{2\omega}, \quad (2)$$

where η_0 is the normalized efficiency, λ is the wavelength of the fundamental light, a_i is the absorption coefficient, β is the two-photon absorption coefficient at the SHG wavelength, and $\Delta k = 4\pi(n_{2\omega} - n_\omega)/\lambda - 2\pi m/\Lambda$ is the phase mismatch, where Λ is the grating period and m is the grating order.

The equilibrium temperature distribution in the waveguide can be described by a 3D Poisson's equation[13]:

$$\nabla^2 T = -q/k, \quad (3)$$

where k is the thermal conductivity and $q = a_\omega I_\omega + a_{2\omega}I_{2\omega} + \beta I_{2\omega}^2$ is the heat source. In the heat source, $I_i = e_i^2(x,y)A_i^2$ is the light intensity.

Although the depletion of the fundamental wave can be neglected in bulk crystal SHG devices, it is not possible in the SHG waveguide devices with high conversion efficiency[14,15]. The finite difference method is adopted to calculate the equilibrium temperature and the SHG

power. The coupling of the light field with temperature is achieved through the temperature-dependent refractive index equations[16]. Grating period is $\Lambda = 7.92$ μm. The corresponding quasi-phase-matching (QPM) temperature is 57.13 °C. Thermal conductivity is k= 4 W/mK. The effective widths of the fundamental (SHG) TM_{00} modal fields in the x and y directions are set as w_{x1}= 5 μm ($w_{x2} = w_{x1}/\sqrt{2}$) and w_{y1}= 5.5 μm ($w_{y2} = w_{y1}/\sqrt{2}$), respectively[12]. Boundary temperature of the waveguide is equal to the QPM temperature. The GRIIRA and two-photon absorption coefficients are different in the waveguides fabricated under different conditions. Therefore, four PPMgLN waveguides with different absorption coefficients are considered[17−20]. Waveguide I is an ultra-low loss waveguide where absorption can be neglected. Waveguide II is a conventional waveguide where a_ω=0.02 cm^{-1}, $a_{2\omega}$=0.04 cm^{-1}, and β=2 cm/GW. Waveguide III has larger linear absorption coefficients where a_ω=0.098 cm^{-1}, $a_{2\omega}$=0.15 cm^{-1}, and β=2 cm/GW. Waveguide IV has the absorption coefficients where a_ω=0.02 cm^{-1}, $a_{2\omega}$=0.04 cm^{-1}, and β=2×10^3 cm/GW. Additionally, the GRIIRA can be neglected for the 5 mol% MgO: $LiNbO_3$ crystal[9]. The normalized efficiency is assumed to be 200% W^{-1}·cm^2. As shown in Fig. 1, the crystals have a length, width, and height of 20, 3, and 0.5 mm, respectively. Waveguides are applied on the top of the crystals with a width of 5 μm and a height of 3 μm. The calculations are performed for 50×35 × 20 000 (μm) regions and discretized into 50×35× 200 point grid for the thermal field, modal envelope, and light intensity. The fundamental laser employed is a continuous wave (CW) laser at 1 111.6 nm with a maximum power of P_ω=1 W. Therefore, the laser intensities inside the waveguide are lower than the photorefractive damage threshold[9].

The functions of the SHG power are calculated versus the fundamental power for the four different waveguides. For each waveguide, the calculations are carried out in three cases, as shown in Fig. 2. First, temperature variations caused by the absorption of light (diamond lines) are taken into account. Second, heat generation is neglected (solid circles). Third, absorptions are neglected (solid line). In waveguide I, the absorptions can be neglected. Therefore, the simulation data are in good agreement with the results of theoretical calculation using $P_{2\omega} = P_\omega \tanh^2(\sqrt{\eta_0 P_\omega})$, as shown in Fig. 2(a). In waveguide II, the simulation and calculation results are in a good agreement with each other when the fundamental wave power is lower than 0.3 W. Discrepancies are observed when the fundamental power is higher than 0.3 W. The SHG power in the calculation is higher than the simulation results. This is the first discrepancy which is caused when the absorptions in the calculation are neglected. Below the fundamental power of 0.3 W, the calculation can provide good approximation of the absorptions by lowering the normalized efficiency. Above 0.3 W, the calculation does not work well and the relation among SHG power, fundamental wave power, and absorptions must be given by a more accurate equation. Two simulation results are different when the fundamental light power is higher than 0.6 W. This is the second discrepancy which is mainly attributed to the thermally induced dephasing. In addition, the saturation of the

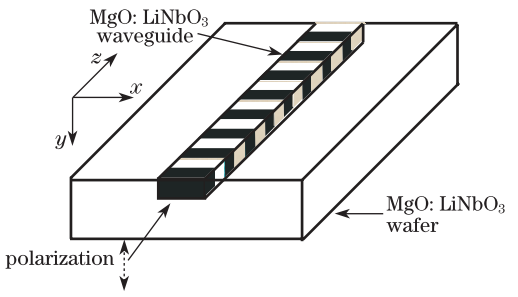

Fig. 1. Optical setup of the SHG in the PPMgLN waveguide.

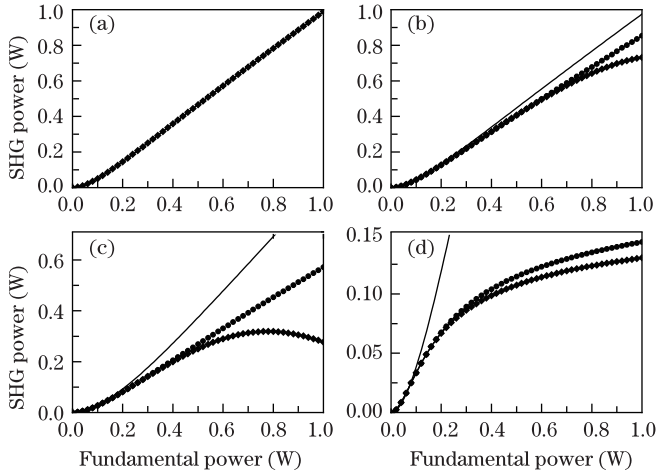

Fig. 2. (a) SHG power versus fundamental light power of waveguide I (diamond lines) obtained by simulations and theoretical calculation (solid line). (b)–(d) SHG power versus the fundamental light power obtained by simulations when the thermal field distributions are considered (diamond figures) and neglected (solid circles), and the theoretical calculations (solid line) of waveguides II–IV.

SHG power has been observed in the fundamental light power higher than 1 W. With increasing absorptions in waveguide III, the discrepancies appear earlier (P_ω >0.2 W). Similarly, the first discrepancy is produced when the absorptions in the theoretical calculation are neglected. The other discrepancy is obtained when the heat generation in one of the simulations is not considered. In waveguide IV, a significant drop-off from the theoretical calculation is observed as the fundamental light power increases to values greater than 0.1 W. The comparison of the three results shows that the dominant effect for the efficiency loss is absorptions under the condition of fundamental light power lower than 0.3 W. Moreover, the thermally induced dephasing occurs when the fundamental light power is greater than 0.3 W. With the large two-photon absorption at the SHG wavelength, the conversion efficiency decreases very rapidly. Figure 2(d) shows that the two-photon absorption is the main effect that reduces the conversion efficiency. The influence of the thermal dephasing is slight. Based on the data of the four waveguides, the drop-off from the theoretical calculation as the fundamental power increases is mainly caused by two effects, namely, absorptions and thermally induced dephasing. To obtain the description of the thermally induced dephasing, the relation among SHG power, fundamental wave power, and absorptions

should be described by a more accurate equation other than the $\tanh^2$ relation.

To investigate the thermally induced dephasing, we calculated the temperature and the power distribution along the beam propagation direction in waveguide III at the fundamental power of 1 W. Figure 3 shows that the waveguide temperature has increased by more than 0.5 °C and the temperature varies along the light propagation axis. The variation is caused by the different fundamental and SHG light absorption coefficients. The temperature increase in the front part of the waveguide is mainly attributed to infrared absorption. In the middle part of the waveguide, the temperature increase is mainly dominated by the SHG absorption. Consequently, the temperature reaches the peak with increasing SHG power. The thermal field changed the refractive index and disturbed the QPM condition. Thus, the SHG power begins to decrease, and the fundamental light power begins to increase. At the end of the waveguide, the SHG power reaches the minimum value. In the case of the high power SHG, a device of proper length can improve the conversion efficiency.

The transverse distribution of the fundamental and SHG intensities and the corresponding temperature distribution at the middle of the waveguide are shown in Fig. 4. A large difference between the QPM temperature and the actual temperature is observed. This is caused by the heat generation of the laser beam. The transverse profiles of the light fields are determined by the refractive index profile of the waveguide. The heat generation of the waveguide is mainly produced by the absorption of the SHG power, and the temperature distributions are different in the x and y directions. By adjusting the waveguide temperature, the SHG power can be corrected partially. However, the loss caused by the axial variation of the temperature cannot be corrected.

In conclusion, we investigate the efficiency loss of the high power SHG in the PPMgLN waveguides. In the lossless waveguide, the capability of theoretical calculation to provide good approximation of the simulation data is demonstrated. In the normal waveguide, significant drop off from the $\tanh^2$ relation is achieved. The final results show that neglecting the absorptions in the $\tanh^2$ relation is the main factor for the drop-off before the onset of the thermally induced dephasing. In addition to absorptions, thermally induced dephasing is the other effect that reduces the conversion efficiency. Heat generation is directly related to the green light absorption at high fundamental powers. In the waveguides with large nonlinear absorption, the efficiency loss is attributed to the nonlinear absorption rather than thermal dephasing. The observation that the thermally induced dephasing starts at different fundamental powers in the PPMgLN waveguides indicates that thermally induced dephasing can be obviated by carefully controlling the crystal growth to reduce light-absorbing defects.

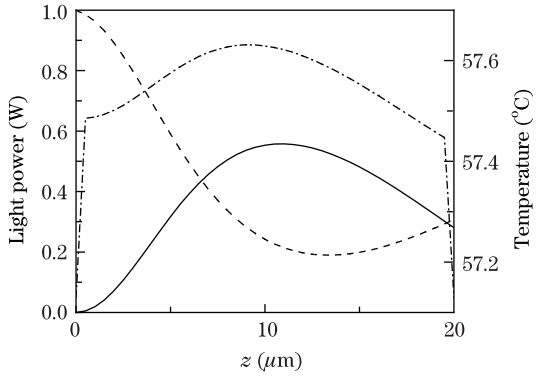

Fig. 3. Final distribution of the fundamental (dashed line) and SHG (solid line) powers along the beam propagation direction with the corresponding temperature distribution (dashed dotted line) at x=25 μm, y=2.5 μm.

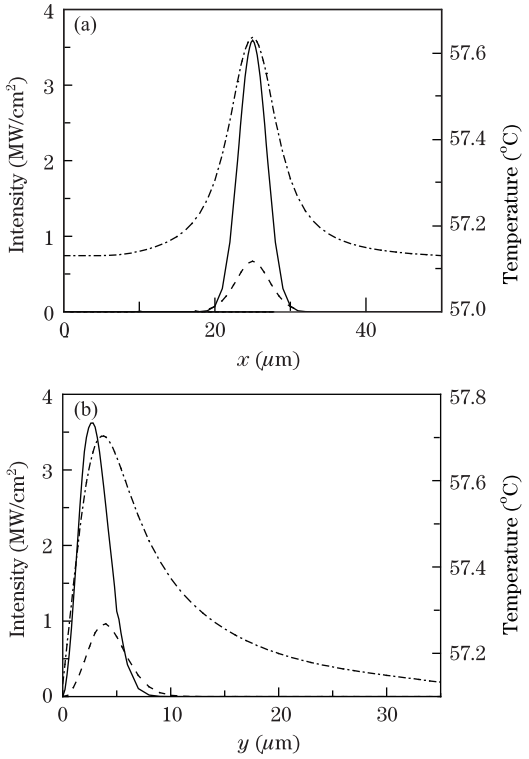

Fig. 4. Intensity distribution of SHG (solid line) and fundamental light (dashed line) in the (a) x and (b) y directions with corresponding temperature distribution (dashed dotted line) in the x (at z=10 000 μm and y=2.5 μm) and y directions (at z=10 000 μm and x=25 μm)

This work was supported by the National Natural Science Foundation of China (Nos. 10774044 and 11134003), the National Key Basic Research and Development Program of China (Nos. 2010CB922903 and 2012CB821302), the Shanghai Pujiang Talent Program of China (No. 07PJ14038), and the PhD Program Scholarship Fund of ECNU 2009 (No. 2009049).

References

1. K. R. Parameswaran, J. R. Kurz, R. V. Roussev, and M. M. Fejer, Opt. Lett. **27,** 43 (2002).
2. K. R. Parameswaran, R. K. Route, J. R. Kurz, R. V. Roussev, M. M. Fejer, and M. Fujimura, Opt. Lett. **27,** 179 (2002).
3. K. SaKai, Y. Koyata, and Y. Hirano, Opt. Lett. **32,** 2342 (2007).
4. A. Jechow, M. Schedel, S. Stry, J. Sacher, and R. Menzel, Opt. Lett. **32,** 3035 (2007).
5. A. Bouchier, G. Lucas-Leclin, P. Georges, and J. M.

Maillard, Opt. Express **13,** 6974 (2005).
6. O. A. Louchev, N. E. Yu, S. Kurimura, and K. Kitamura, Appl. Phys. Lett. **87,** 131101 (2005).
7. Z. M. Liao, S. A. Payne, J. Dawson, A. Drobshoff, C. Ebbers, and D. Pennington, J. Opt. Soc. Am. B **21,** 2194 (2004).
8. F. J. Kontur, I. Dajani, Y. Lu, and R. J. Knize, Opt. Express **15,** 12882 (2007).
9. K. Furukawa, K. Kitamura, A. Alexandrovski, R. K. Route, M. M. Fejer, and G. Foulon, Appl. Phys. Lett. **78,** 1970 (2001).
10. F. Ji, R. Lu, B. Li, B. Zhang, and J. Yao, Chin. Opt. Lett. **8,** 505 (2010).
11. X. Wei, Y. Peng, W. Wang, and X. Chen, Chin. Opt. Lett. **8,** 1061 (2010).
12. P. F. Hu, T. C. Chong, L. P. Shi, and W. X. Hou, Opt. Quant. Electron. **31,** 337 (1999).
13. D. Eimerl, IEEE J. Quantum Electron. **23,** 2238 (1987).
14. M. M. Fejer, G. A. Magel, D. H. Jundt, and R. L. Byer, IEEE J. Quantum Electron. **28,** 2631 (1992).
15. R. C. Eckardt and J. Reintjes, IEEE J. Quantum Electron. **10,** 1178 (1984).
16. O. Gayer, Z. Sacks, E. Galun, and A. Arie, Appl. Phys. B **91,** 343 (2008).
17. B. M. Jin, I. W. Kim, W. B. White, and A. S. Bhalla, Mater. Lett. **30,** 385 (1997).
18. R. K. Choubey, P. Sen, P. K. Sen, R. Bhatt, S. Kar, V. Shukla, and K. S. Bartwal, Opt. Mater **28,** 467 (2006).
19. F. Charra, G. Gurzadyan: *A-D.* D. F. Nelson, (ed.). SpringerMaterials-The Landolt-Börnstein Database (http://www.springermaterials.com). DOI:10.1007/1013-4958_40.
20. L. Pàlfalvi, G. Almási, J. H. Ágnespéter, and K. Polgár, Appl. Phys. Lett. **80,** 2245 (2002).